Realistic Partial State Densities for Proton-Neutron Configurations in Nuclei near Closed Shells

K. Albrecht and M. Blann

Department of Chemistry, and Nuclear Structure Research Laboratory, University of Rochester, Rochester, New York 14627

(Received 31 May 1973)

Using Nilsson single-particle level schemes as input, we have calculated partial state densities for excited proton-neutron configurations with specified particle-hole numbers. The recursion relation method used is general and free of any mathematical approximations. Results are given for nuclides in the Sn region and for several Pb isotopes. The strong shell effects in these nuclei are clearly reflected in their state densities. The results are compared to densities obtained from the equidistant-spacing model. This model not only fails completely at low excitation energies as expected, but it also disagrees in several cases with the average behavior of the realistic densities at higher energies.

1. INTRODUCTION

The need for calculations of realistic state densities in connection with the preequilibrium decay model[1] has been emphasized in a previous paper[2] to which the reader is referred for further details. While only one kind of fermions (protons) was considered in Ref. 2, we describe in this work state density calculations for configurations with specified numbers of excited particles and holes for both kinds of nucleons. This enables us to investigate the dependence of the state density for particle-hole (p-h) configurations on both shell effects and its composition in terms of proton and neutron numbers.

The partial state densities are obtained from realistic single-particle level schemes, using a method which is mathematically exact. Its key element is a recursion relation described earlier[3,4] for the case of total state densities, i.e., those summed over all p-h configurations. The method has been applied to proton p-h states in Ref. 2, but as some improvements have been included we feel that a more detailed discussion of the p-h recursion relation technique is in order.

The realistic results will then be compared with densities obtained from the equidistant-spacing model (ESM) for the single-particle levels. As the ESM obviously contains no shell structure, it is bound to fail for near-magic nuclei at low excitation energies. For higher excitations, however, the ESM total state density (i.e., Bethe's formula) is found[4] to approximate the realistic total density reasonably well if an energy-shift parameter is included. Since in this paper the total density is broken down into partial contributions from each p-h configuration, we can investigate the role of the ESM in greater detail.

2. CLASSIFICATION OF EXCITED PARTICLES AND HOLES

In order to define the notation used in this work we first state what we mean by a particle-hole configuration for one kind of fermion. Let the single-particle states $|i\rangle$ be numbered in ascending order of their energies ϵ_i. Thus in the ground state of a system having N particles total, all states with $\epsilon_1, \ldots, \epsilon_N$ will be occupied. Now the usual way to classify excited particles (see, e.g., Ref. 5, Sec. 3B-1) is to count the number of occupied orbits with $i > N$. This number is, of course, equal to the number of holes. This well-known scheme is illustrated in the left column of Fig. 1. Each state is represented by one level, although in actual cases the levels will be degenerate. Particles (holes) can then be visualized as occupied (unoccupied) states "above" ("below") the Fermi energy ϵ^F. Such configurations defined with respect to ϵ^F will be labeled $0P0H$, $1P1H$, $2P2H$, etc.

The above scheme is, however, not appropriate for classification of the series of p-h configurations arising from incident particles captured (temporarily) in a nucleus. Let us assume two incident particles on a target having $(N-2)$ particles (e.g., the proton part of an α-induced reaction). As shown in Fig. 1, the initial configuration of the compound system is either $2P2H$ (with two holes fixed just below ϵ^F) or $1P1H$ (the hole being in ϵ_N or ϵ_{N-1}) or the ground state $0P0H$. Thus the initial configuration belongs to subsets of three different P-H classes, which is inconvenient.

We therefore do not classify particles and holes with respect to ϵ^F, but use instead the target Fermi energy ϵ^R as our reference energy. Denoting the new classes with small letters, the initial configuration in Fig. 1 is now labeled simply $2p$. The

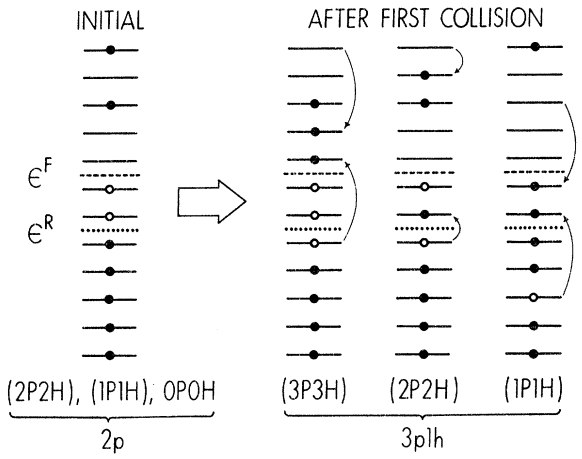

FIG. 1. Classification schemes for particle-hole excitations. At left, a compound system is formed by two incident particles. After the first two-body interaction has occurred, the system is either still in the same configuration class or in one of the classes shown on the right side. Classification with respect to the energies ϵ^F and ϵ^R is defined in Sec. 2.

same simplification obtains for higher exciton numbers. After the first two-body interaction has occurred, the system is either still in the 2*p* class or in the 3*p*1*h* class (see Fig. 1, right side). In the conventional scheme, the latter configurations belong to (subsets of) the 3*P*3*H*, 2*P*2*H*, or 1*P*1*H* classes.

The classification with respect to ϵ^R obviously depends on how the compound system was formed, since the number of states between ϵ^F and ϵ^R is equal to the number $\mathcal{P}^{\rm inc}$ of incident particles. Therefore, it reflects more closely the configurations during the equilibration process via successive two-body interactions as is required in preequilibrium decay models.

3. CALCULATION OF PARTIAL STATE DENSITIES FROM REALISTIC SINGLE-PARTICLE LEVELS

In order to write down the recursion relations for the density ω of particle and hole states for one kind of fermion, we measure the single-particle (-hole) energies from ϵ^R; thus

$$\epsilon_i^{\rm part} = \epsilon_{i+N-\mathcal{P}^{\rm inc}} - \epsilon^R$$

and

$$\epsilon_i^{\rm hole} = \epsilon^R - \epsilon_{N-\mathcal{P}^{\rm inc}+1-i} \ .$$

If the total energies are also measured from ϵ^R, the ground-state energy for all hole configurations is $E_0^{\rm hole}=0$, while the particles' ground-state energy depends on their number $\mathcal{P}$ as

$$E_0^{\rm part} = \sum_{i=1}^{\min(\mathcal{P},\mathcal{P}^{\rm inc})} \epsilon_i^{\rm part} \ .$$

In analogy to Sec. 2 of Ref. 3 we then obtain the recursion relation in terms of the excitation energies Q ($Q^{\rm part}=E^{\rm part}-E_0^{\rm part}$, $Q^{\rm hole}=E^{\rm hole}$) as

$$\omega_i(\mathcal{P},Q) = \omega_{i-1}(\mathcal{P},Q) + \omega_{i-1}(\mathcal{P}-1,\ Q+\Delta(\mathcal{P})-\epsilon_i^{\rm part}) \tag{1}$$

for particles and

$$\omega_i(\mathcal{H},Q) = \omega_{i-1}(\mathcal{H},Q) + \omega_{i-1}(\mathcal{H}-1,\ Q-\epsilon_i^{\rm hole}) \tag{2}$$

for holes.

The recursion starts with $\omega_0(n,Q)=\delta_{n0}\delta_{Q0}$. (The energy variable must be discretized in bins of suitable size since the recursion is carried out numerically.) The correction term

$$\Delta(\mathcal{P}) = E_0^{\rm part}(\mathcal{P}) - E_0^{\rm part}(\mathcal{P}-1) = \begin{cases} 0 & \text{if } \mathcal{P} \geqslant \mathcal{P}^{\rm inc} \\ \epsilon_{\mathcal{P}}^{\rm part} & \text{if } \mathcal{P} < \mathcal{P}^{\rm inc} \end{cases} \tag{3}$$

accounts for the energy difference between the ground states of the $\mathcal{P}$ and $(\mathcal{P}-1)$ particle systems. This term was neglected in Ref. 2 although its effect turns out to be appreciable near a major shell gap. With each recursion step i, the corresponding state with ϵ_i enters the density calculation. Realizing this, Eqs. (1) and (2) can be proved immediately by induction without recourse to the grand partition function technique of Ref. 3. Consider, e.g., relation (1) which is obviously correct for $i=1$. Now assume that for a spectrum consisting of $(i-1)$ single-particle states the density ω_{i-1} is known for all $\mathcal{P}$ and Q. For each $\mathcal{P}$, the inclusion of the state $|i\rangle$ leads to new $\mathcal{P}$ states only if it is occupied, of course. This leaves $Q_r = Q + \Delta(\mathcal{P}) - \epsilon_i^{\rm part}$ units of excitation energy for the remaining $(\mathcal{P}-1)$ particles. If Q is such that the latter system has a number of states at Q_r, the same number of states is gained by the $\mathcal{P}$ particle system at Q from the inclusion of $\epsilon_i^{\rm part}$.

For any finite number of particles (holes) and finite excitation Q, the final values $\omega(\mathcal{P},Q)$ and $\omega(\mathcal{H},Q)$ are reached in a finite number of recursion steps. The state density of a p-h configuration is then given by the sum over all (discrete) energy partitions

$$\omega(\mathcal{P},\mathcal{H},Q) = \sum_{U=0}^{Q} \omega(\mathcal{P},U)\omega(\mathcal{H},Q-U) \ . \tag{4}$$

So far we have considered only one kind of fermion. If both protons and neutrons can share the excita-

tion, we calculate $\omega(\mathcal{P}_\pi, \mathcal{H}_\pi, Q)$ and $\omega(\mathcal{P}_\nu, \mathcal{H}_\nu, Q)$ from their level schemes. Folding once more, we finally arrive at the density of states with $\mathcal{P}_\pi$ protons, $\mathcal{H}_\pi$ proton holes, $\mathcal{P}_\nu$ neutrons, and $\mathcal{H}_\nu$ neutron holes at excitation E_x:

$$\omega(\mathcal{P}_\pi, \mathcal{H}_\pi, \mathcal{P}_\nu, \mathcal{H}_\nu, E_x) = \sum_{Q=0}^{Ex} \omega(\mathcal{P}_\pi, \mathcal{H}_\pi, Q) \times \omega(\mathcal{P}_\nu, \mathcal{H}_\nu, E_x - Q) . \tag{5}$$

The present results have been calculated with the same input parameters as those in Ref. 2, except that the excitation energy range is now 0–40 MeV, at 0.1-MeV increments. The single-particle energies are again generated from Nilsson's 1955 Hamiltonian.[6] This means that the same set of levels is used for protons and neutrons, although the computer code is arranged so that it can handle different arbitrary sets. All results presented herein are for zero deformation, but arbitrary deformation may be specified as input to the code.

To simulate residual interactions and to smoothen the results, the densities (5) were averaged with a Gaussian function of 0.3-MeV width. This smoothing, of course, in no way accounts for the pairing interaction, the effects of which depend on the excitation energy as well as on the number of excitons. Unfortunately no method has yet been found to include pairing in the recursion technique while maintaining its exactness and simplicity. Only under the assumption of purely diagonal pairing (which is not justified in the present case) has a suitable recursion relation been established.[3]

4. PARTIAL STATE DENSITIES FROM THE EQUIDISTANT-SPACING MODEL

Since the ESM leads (in good approximation) to a simple analytical expression for the partial state density, it has been used in all preequilibrium calculations. It is therefore interesting to compare the realistic densities with those derived from the ESM. We use an expression for ω^{ESM} obtained by Williams[7] and rewrite it in the following way:

$$\omega^{\mathrm{ESM}}(\mathcal{P}_\pi, \mathcal{H}_\pi, \mathcal{P}_\nu, \mathcal{H}_\nu, E_x) = \frac{\tilde{g}(\tilde{g}E_x - \tilde{\theta})^{\mathfrak{N}-1}}{\mathcal{P}!\,\mathcal{H}!\,(\mathfrak{N}-1)!} , \tag{6}$$

where $\mathcal{P} = \mathcal{P}_\pi + \mathcal{P}_\nu$ is the total number of excited particles and $\mathcal{H} = \mathcal{H}_\pi + \mathcal{H}_\nu$ the total number of holes. Further, $\mathfrak{N} = \mathcal{P} + \mathcal{H}$ is the total exciton number. The proton-neutron partial state density is thus expressed as the density of an equivalent one-fermion system having effective single-particle state density $\tilde{g}$ and effective shift $\tilde{\theta}$. Only these quantities depend on the composition of the actual system:

$$\tilde{g} = \left[\binom{\mathcal{P}}{\mathcal{P}_\pi} \binom{\mathcal{H}}{\mathcal{H}_\pi} g_\pi^{\mathcal{P}_\pi + \mathcal{H}_\pi} g_\nu^{\mathcal{P}_\nu + \mathcal{H}_\nu} \right]^{1/\mathfrak{N}} \tag{7}$$

and

$$\tilde{\theta} = \tilde{g} \left(\frac{\theta_\pi}{g_\pi} + \frac{\theta_\nu}{g_\nu} \right) , \tag{8}$$

with

$$\theta_\pi = \tfrac{1}{4}(\mathcal{P}_\pi^{\,2} + \mathcal{H}_\pi^{\,2}) + \tfrac{1}{4}(\mathcal{P}_\pi - \mathcal{H}_\pi) - \tfrac{1}{2}\mathcal{H}_\pi . \tag{9}$$

The analogous formula holds for the neutron shift θ_ν. In these equations, g_π and g_ν are the single-proton and -neutron state densities, respectively. It is seen that the effective density $\tilde{g}$ is slightly larger than the weighted geometric mean of g_π and g_ν. When ω^{ESM} is summed over all proton-neutron compositions having a total of $\mathcal{P}$ particles and $\mathcal{H}$ holes, the result is again Eq. (6) with $\tilde{g} = g_\pi + g_\nu$, as expected, aside from minor discrepancies in the $\tilde{\theta}$ term, which is numerically small, however.

Though g_π and g_ν are, in principle, independent parameters of the ESM, they are usually expressed in terms of only one spacing parameter d as $g_\pi = Z/d$, $g_\nu = N/d$. This form is suggested by the Fermi-gas model, which yields a constant value $d_F = \frac{2}{5}\epsilon_F \approx 25$ MeV for all nuclei (see, e.g., Ref. 5, Sec. 2-I for details).

For later use we note that the density ratio for two configurations differing only by the exchange of one proton p-h pair into a neutron p-h pair is given by

$$\frac{\omega(\mathcal{P}_\pi + 1, \mathcal{H}_\pi + 1, \mathcal{P}_\nu - 1, \mathcal{H}_\nu - 1, E_x)}{\omega(\mathcal{P}_\pi, \mathcal{H}_\pi, \mathcal{P}_\nu, \mathcal{H}_\nu, E_x)} = \frac{\mathcal{P} - \mathcal{P}_\pi}{\mathcal{P}_\pi + 1} \frac{\mathcal{H} - \mathcal{H}_\pi}{\mathcal{H}_\pi + 1} \left(\frac{g_\pi}{g_\nu} \right)^2 . \tag{10}$$

Here we have neglected the small θ terms. More generally, the ratio of any two ω's having the same total $\mathfrak{N}$ is independent of the excitation, except for very small E_x. For given $\mathcal{P}$ and $\mathcal{H}$ the dominant configuration (6) can be found from Eq. (10) by solving for those values of $\mathcal{P}_\pi$ and $\mathcal{H}_\pi$ which bring its right-hand side closest to unity.

5. RESULTS AND DISCUSSION

In the following we shall label a proton-neutron particle-hole configuration as $p^{\mathcal{P}_\pi} p^{-\mathcal{H}_\pi} n^{\mathcal{P}_\nu} n^{-\mathcal{H}_\nu}$. A proton-induced reaction is assumed throughout this paper. Thus we have the configurations p, nn^{-1}, p^2p^{-1}, pnn^{-1}, p^3p^{-2}, $p^2p^{-1}nn^{-1}$, pn^2n^{-2}, limiting ourselves to a maximum of five excitons total. The computer code can handle any arbitrary configurations. The limited choice is to illustrate the

effects resulting from realistic single-particle levels, and is not intended as an exhaustive set of results.

A. Tin Region

The first group of results in Figs. 2 and 3 is for the compound nuclei $Z=46$, 48, 50, 52 with $A=115$, for which pure proton configuration state densities were given in Ref. 2. Comparing the present p^2p^{-1} and p^3p^{-2} results to those of the earlier paper we are thus able to see the influence of the neglected correction term Δ given in Eq. (3) near a major shell closure. All curves are shifted appreciably to the left with respect to those in Ref. 2, causing a smaller intercept with the E_x axis. The wiggle topology has also changed considerably in some cases. The qualitative behavior of the pure proton densities is, however, similar to the earlier results. As the shell closure is approached ($Z=46$, 48) the state density at low excitation drops sharply and goes through its minimum at $Z=50$. Above the closure ω recovers rapidly, as many single-proton states become available.

The single-proton state density $\omega_p=\omega(1, 0, 0, 0, E_x)$ is plotted in Fig. 2 for $Z=46$. For the other nuclides, ω_p is obtained simply by shifting the energy scale. Due to the large shell gap of 3.5 MeV at $Z=50$, ω_p has a deep minimum at $E_x=0$. The other minima at $E_x=8$ and 14 MeV are due to the $Z=82$ and 126 closures. The ω_p curve gives also an impression of the effects of the smoothing procedure applied to the realistic results.

Let us now consider configurations involving neutrons as well as protons. The density for the lowest neutron configuration $\omega_{nn^{-1}}$ is shown in Fig. 2 for $N=63$. Around $E_x=0$ this density is small, due to the minor shell gap at $N=64$. It then quickly rises to its average value, interrupted only by a steep minimum caused by the $N=82$ gap at $E_x\approx 4$ MeV. Thus the excited neutron configurations essentially start from a mid-shell situation, which is clearly reflected in Figs. 2 and 3.

When in a pure proton configuration one pp^{-1} pair is converted into an nn^{-1} pair (e.g., $p^2p^{-1}\rightarrow pnn^{-1}$) the density in general becomes considerably larger and smoother and the energy intercept decreases. For excitations which are not too low, this increase in magnitude is easily seen to result from two causes. The average single-neutron density is higher than the average single-proton density and the number of distinguishable configurations rises when the other kind of fermion is first introduced.

If the exciton number is large enough, a second pair pp^{-1} can be converted to nn^{-1}, such as for $p^2p^{-1}nn^{-1}\rightarrow pn^2n^{-2}$ in Fig. 3. In this case, the effect of $g_\nu > g_\pi$ is counteracted by the decreasing number of distinguishable configurations (which peaks, of course, at $\mathcal{P}_\pi=\mathcal{P}_\nu=\frac{1}{2}\mathcal{P}$, $\mathcal{H}_\pi=\mathcal{H}_\nu=\frac{1}{2}\mathcal{H}$). The net outcome is therefore less predictable,

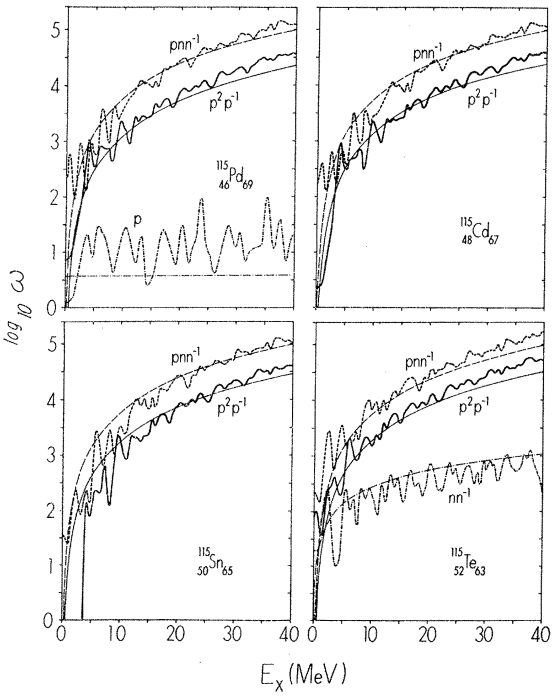

FIG. 2. Partial state densities ω (in units of MeV^{-1}) for 1-, 2-, and 3-exciton configurations in the Sn region as function of the excitation energy. The smooth curves are ESM results.

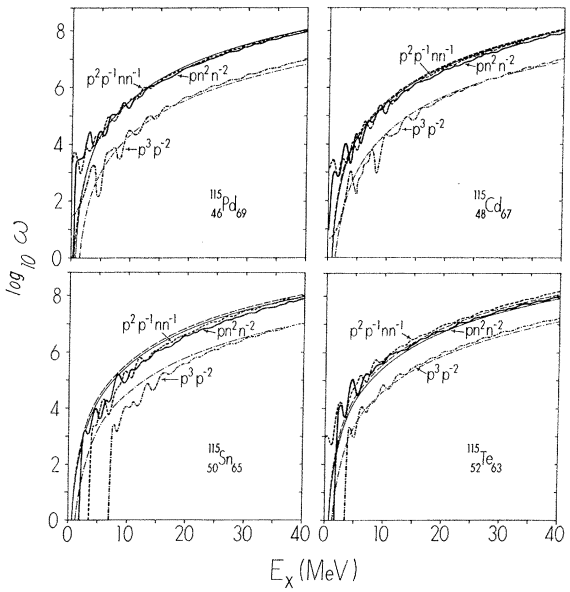

FIG. 3. The same as Fig. 2 for 5-exciton configurations.

but it turns out (Fig. 3) that in our cases the two effects cancel nearly exactly at higher excitations, i.e., $\omega_{p^2p^{-1}nn^{-1}} \approx \omega_{pn^2n^{-2}}$. The average difference of $\log\omega$ at high excitations for two configurations having the same $\mathfrak{N}$ is reproduced surprisingly well by the ESM formula (10). For small E_x, however, the regularities described above no longer hold and the density structure is determined by the individual level structure of each nuclide.

B. Lead Isotopes

Shell effects in the state density will be most pronounced for a double shell closure. This is demonstrated in Fig. 4, where the (total) proton number is kept fixed at $Z = 82$, while N varies around 126. Consequently, the proton contribution to the density does not change with N, as the smooth A dependence of Nilsson's levels can be neglected over the small range of A considered here. Thus Fig. 4 complements Figs. 2 and 3 in the following sense: It shows the variation of the neutron shell effect near a shell closure in the presence of a large (but constant) proton shell effect, while Figs. 2 and 3 show the behavior near a single shell closure with the other kind of fermion occupying the middle of a major shell.

Due to the higher density of single-particle levels in Pb, the partial densities fluctuate much less than those in the Sn region. For large E_x the same regularities in the average behavior of ω as discussed in the previous subsection are seen to hold here. Even for small E_x, a regularity is observed now: For each exciton number (3 or 5) the most neutron-rich configuration has the highest density. This is not simply due to the fact that the neutron shell gap (2 MeV) is smaller than the proton gap (3.5 MeV). It also results from the number of single-particle states available above and below the gaps. Otherwise Figs. 2 and 3 would exhibit this regularity as well.

Except for the very neutron-rich configurations in ^{210}Pb, all energy intercepts in Fig. 4 are of considerable magnitude, as expected near a double shell closure. Thus the discrepancy with respect to ω^{ESM} is very large for small excitations and can reach six orders of magnitude in the most unfavorable case.

C. Comparison to ESM Results

The only free ESM parameter is the spacing d introduced in Sec. 4. Its value practically does

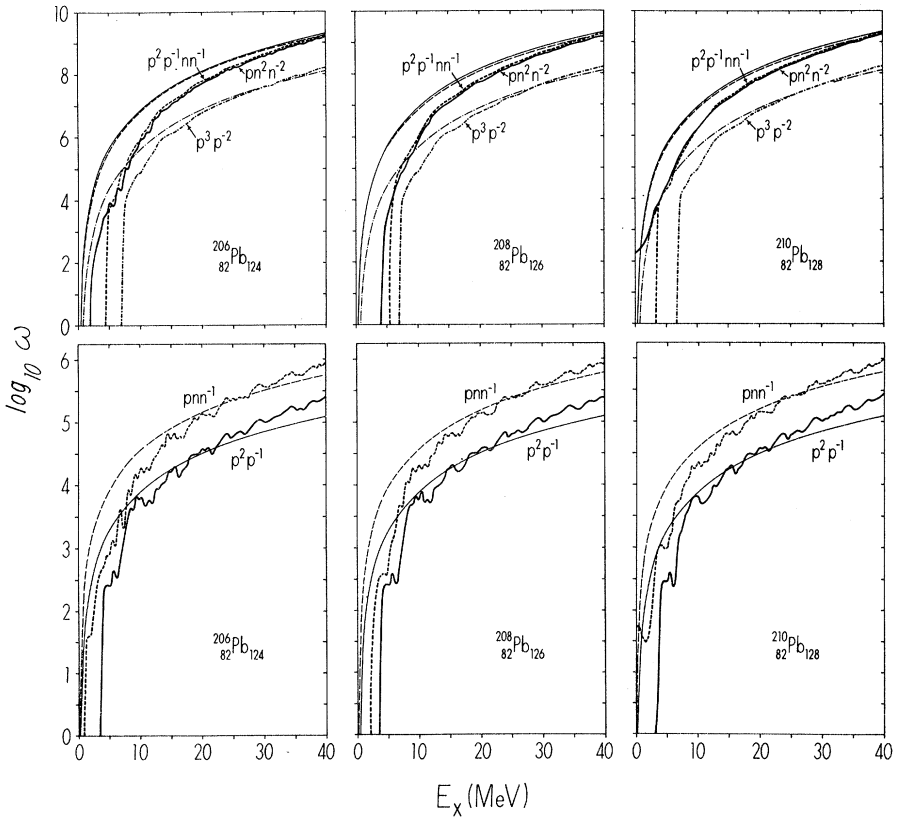

FIG. 4. The same as Figs. 2 and 3, but for Pb isotopes.

not influence the shape of the curve $\log\omega^{\mathrm{ESM}}(E_x)$, since $d\log\omega^{\mathrm{ESM}}/dE_x = (\mathfrak{N}-1)/E_x$, neglecting the small effect of the $\tilde{\theta}$ term. Thus varying d will merely result in a vertical shift of the curve. The same holds true if g_π and g_ν are treated as independent parameters.

The value of d is chosen here such that ω^{ESM} fits the average behavior of the realistic ω at high excitation as well as possible. For both the Sn and the Pb region we found $d = 12$ MeV satisfactory. This value differs from the $d = 14$ MeV used in Ref. 2, due to the fact that the increased range of E_x considered here (40 MeV vs 20) allows us to determine d more precisely. Part of the discrepancy may also result from the Δ term neglected earlier. The spacing d is related to the more familiar level density parameter a by

$$a = \frac{\pi^2}{6}(g_\pi + g_\nu) = \frac{\pi^2}{6}\frac{A}{d} ,$$

which yields $a = A/7.3$ MeV^{-1} for our choice of d. Thus $a = 15.8$ MeV^{-1} for the Sn region and $a = 28.5$ MeV^{-1} for Pb. Both numbers agree reasonably well with those obtained by Williams, Chan, and Huizenga,[4] who fitted the ESM total state density expression (back-shifted Fermi-gas formula) to recursion-relation results in the 40–60-MeV range. The Pb value is also in agreement with the experimental data taken at these energies (see Ref. 4 for a fuller discussion). It differs, however, drastically from the value $a \approx 11$ MeV^{-1} found at low excitations in Pb [see, e.g., the $a(A)$ data in Ref. 8], due to the washing out of shell effects with increasing E_x.

This behavior of a seems to be most characteristic for a double shell closure, since it is not observed in the Sn region. Here, our value of a is practically the same as the one obtained from experiments at low energies. Thus the effect of the proton shell $Z = 50$ seems to be overridden by the neutrons as far as a is concerned. This can also be seen from the experimental $a(A)$ curve, which deviates markedly from its average trend $a = A/8$ MeV^{-1} in the vicinity of ^{208}Pb, but not in the Sn region. It should be remembered, however, that this applies only to comparisons made in terms of the over-all parameter a. When the total density is broken down into its partial contributions, the single-shell effect is clearly recognized: The pure proton configurations for ^{115}Sn in Figs. 2 and 3 are those least well approximated by the ESM.

Another ESM feature is also evident from Fig. 2: The discrepancy between realistic and ESM results becomes larger when the exciton number decreases. Thus the average single-proton density (^{115}Pd in Fig. 2) is not reproduced at all by the ESM, because g_π is an average of the densities of excited single-particle and single-hole states, the latter being much smaller than the former. The density ω_{nn-1} is therefore much better reproduced by the ESM, although ω^{ESM} generally overestimates the realistic ω.

For the 3- and 5-exciton configurations in Figs. 2 and 3 the ESM describes the average high-energy behavior of the realistic densities fairly well. This might at first seem surprising since the ESM obviously cannot take into account the increase of the real single-particle density with excitation, but it must be realized that the hole state density decreases with excitation (in fact, there are no hole states above ≈ 30 MeV), therefore these trends cancel partially as soon as holes are present. This cancellation becomes, however, less effective when A is large, because the maximum hole energy does not change appreciably with increasing A, while the increase of the single-particle density g becomes more rapid. (For oscillator potentials $g(\epsilon)$ is roughly proportional to $\epsilon^2 A$.) This is clearly seen in Fig. 4: The slope of $\log\omega^{\mathrm{ESM}}$ (which does not depend on parameters) is consistently smaller than the average slope of the logarithm of the realistic densities.

6. CONCLUSIONS

Partial state densities calculated from realistic level schemes show strong shell effects in nuclei near closed shells. At low and moderate excitations, these densities can differ drastically from those calculated with the ESM. If the latter model is still to be used in the context of preequilibrium decay calculations, we feel that several modifications must be made in the ESM. Such corrections should include independent parameters for the average single-particle density as well as for the single-hole density. Most crucial near closed shells is the introduction of an energy-shift parameter depending on the number of excitons and the difference between the actual and the average single-particle density of states at the Fermi energy. Finally, the shape parameter $\mathfrak{N}$ of the $\log\omega$ curve should be made adjustable to include the effects resulting from the variation of the single-particle level density with excitation.

We stress that the above criticism of the ESM is not meant to discredit its value, which lies in its simplicity and generality. The ESM and our approach should rather be regarded as complementary, in that the ESM illuminates the physics of the problem while the realistic density is more appropriate quantitatively, in particular for nuclei near closed shells.

We acknowledge several helpful discussions with Professor J. R. Huizenga.

*Work supported by the U. S. Atomic Energy Commission and the West German Bundesministerium für Forschung und Technologie.

[1]M. Blann, in Proceedings of the Europhysics Conference on Intermediate Processes, Plitvice, Yugoslavia, September 1972, edited by N. Cindro and T. Mayer-Kuckuk (Springer-Verlag, to be published).

[2]F. C. Williams, Jr., A. Mignerey, and M. Blann, Nucl. Phys. A207, 619 (1973).

[3]F. C. Williams, Jr., Nucl. Phys. A133, 33 (1969).

[4]F. C. Williams, Jr., G. Chan, and J. R. Huizenga, Nucl. Phys. A187, 225 (1972).

[5]A. Bohr and B. R. Mottelson, *Nuclear Structure* (Benjamin, New York, 1969), Vol. I.

[6]S. G. Nilsson, K. Dan. Vid. Selsk. Mat.-Fys. Medd. 29, No. 16 (1955).

[7]F. C. Williams, Jr., Nucl. Phys. A166, 231 (1971).

[8]J. R. Huizenga, in *Statistical Properties of Nuclei,* edited by J. B. Garg (Plenum, New York, 1969), p. 425.